[Supporting Information]

Towards the Design of a Hierarchical Perovskite Support: Ultra Sintering-Resistant Gold Nanocatalysts for CO Oxidation

Chengcheng Tian, Xiang Zhu, Carter W. Abney, Xiaofei Liu, Guo Shiou Foo, Zili Wu, Meijun Li, Harry M. Meyer III, Suree Brown, Shannon M. Mahurin, Sujuan Wu, Shi-Ze Yang, Jingyue (Jimmy) Liu, and Sheng Dai**

Dr. C.C. Tian, Dr. X. Zhu, X. F. Liu, Dr. M. J. Li, Dr. S. Brown, Prof. S. Dai
Department of Chemistry, University of Tennessee-Knoxville
Knoxville, TN 37996-1600, USA
Email: **xiang@utk.edu (zhuxiang.ecust@gmail.com)**

Dr. C. W. Abney, Dr. S. M. Mahurin, Dr. G. S. Foo, Dr. Z. L. Wu, Prof. S. Dai
Chemical Sciences Division, Oak Ridge National Laboratory
Oak Ridge, TN 37831, USA, Fax: (+1) 865-576-5235
Email: **dais@ornl.gov**

Dr. H. M. Meyer III and S. Z. Yang
Materials Science and Technology Division, Oak Ridge National Laboratory
Oak Ridge, TN 37831, USA

Dr. S. J. Wu
Electron Microscopy Center of Chongqing University, College of Materials Science and Engineering, Chongqing University
Chongqing 400044, China

Prof. J. Liu
Department of Physics, Arizona State University
Tempe, Arizona 85287-1504, USA

Contents

1. Experimental Section

1.1 Preparation of $LaFeO_3$-MCF

Mesostructured cellular foam (MCF) was synthesized as described by Schmidt-Winkel et al.[1] $La(NO_3)_3$ $6H_2O$ (0.165 mmol) and $Fe(NO_3)_3$ $9H_2O$ (0.165 mmol) were dissolved in dilute HNO_3 under vigorous stirring, the pH value of the solution was kept between two and three. Then 10 ml of water-ethanol (v/v=1:7) solution containing citric acid (0.66 mmol) as a chelating agent for the metal ions. The molar ratio of metal ions to citric acid was 1:2. As a cross-linking agent, ethylene glycol was added with a final concentration of 0.20 g ml^{-1}. The solution was stirred for 2 h to form a sol, and then the MCF (0.2 g) was added under stirring. The suspension was further stirred for another 4 h, and then the temperature was then increased to 70 °C and placed under vacuum to completely evaporate solution. Then the dried samples were heated to 500 ◦C with a heating rate of 1 ◦C min^{-1}, and held there for 2 h in air and was further heated to 700 ◦C for 2 h in air with a heating rate of 1 ◦C min^{-1}.

1.2 Synthesis of gold catalysts supported on $LaFeO_3$-MCF

The Au precursor was introduced onto the $LaFeO_3$-MCF support using a deposition-precipitation (DP) method.[2] Typically, 0.01 g of hydrogen tetrachloroaurate (III) trihydrate ($HAuCl_4 \cdot 3H_2O$) was dissolved into 4 mL deionized water. The pH value of the resulting solution was adjusted to 10 using a solution of 1.0 mol L^{-1} NaOH under vigorous stirring at room temperature. Subsequently, the as-synthesized $LaFeO_3$-MCF support was added and the pH value was controlled at 10 by the further addition of NaOH solution. The mixed solution was stirred for an additional 2 h in an 80 °C water bath. Finally, the precipitates were separated by centrifugation and washed several times with deionized water. The product was dried at 50 °C in vacuum overnight to obtain the as-synthesized catalyst.

1.3 Characterization

The powder X-ray diffraction (XRD) data were recorded with a PANalytical Empyrean diffractometer, operated at 45 kV and 40 mA (scanning step: 0.02 ° per step). The diffraction patterns were recorded in the range of 10–80° 2θ. The nanoparticle size (d_{Ba}, nm) was estimated according to Scherrer equation:

$d_{Ba} = K \cdot \lambda / (\beta \cdot \cos\theta)$ ($K = 0.9$, $\lambda = 0.1540598$ nm)

where K is the shape factor, λ is the X-ray wavelength, β is the line broadening at half the maximum intensity (FWHM) in radians, and θ is the Bragg angle. The nitrogen adsorption and desorption isotherms were measured at 77 K under a Gemini 2375 surface area analyzer. Transmission electron microscope (TEM) and Z-contrast scanning transmission electron microscope (STEM) experiments were conducted on HITACH HD2000 microscopes with an accelerating voltage of 200 kV. Elemental analysis of the samples was done by inductively coupled-plasma atomic emission spectroscopy (ICP-AES) using Optima 2100 DV spectrometer (PerkinElmer Corporation). X-ray photoelectron spectroscopy (XPS) measurements: XPS experiments were performed with a PHI 3056 spectrometer equipped with an Al anode source operated at 15 KV and an applied power of 350 W and a pass energy of 93.5 eV.

X-ray absorption fine structure (XAFS) samples were prepared by grinding samples of perovskite with a mortar and pestle to achieve a uniform particle size of < 5 μm. Approximately 10 mg of each sample were loaded one at a time into a six-barrel sample holder, then pressed into a self-supported pellet. The sample holder was enclosed in a quartz tube sealed on each end with stainless steel caps with Mylar windows. Samples were processed and measured under environmental atmosphere.

XAFS investigations were performed at beamline 10ID-B of the Advanced Photon Source at Argonne National Laboratory.[3] Spectra were collected at the gold L_{III}-edge (11919 eV) using a Lytle-type fluorescence detector. A gold foil was measured before and after each series of samples for energy calibration as well as for data analysis. The x-ray white beam was monochromatized by a Si(111) monochromater with higher-order harmonics removed through use of a Rh harmonic rejection mirror. The incident beam intensity (I_0), transmitted beam intensity (I_t) and reference (I_{ref}) were all measured by 20 cm ionization chambers with gas compositions of 95% N_2 and 5% Ar, 10% N_2 and 90% Ar, and 5% N_2 and 95% Ar, respectively. All spectra were collected at room temperature. Samples were centered on the beam and adjusted to find the most homogeneous location for data collection. Due to the high flux

and configuration of the beamline, the x-ray energy was varied at a constant rate across the absorption edge; neither step size nor dwell time changed as a function of energy. Six scans were collected for 0.6 wt% Au $LaFeO_3$, while only three scans were necessary to achieve appropriate signal to noise for 1.0 wt% Au $LaFeO_3$.

Data were processed and analyzed using the Athena and Artemis programs of the IFEFFIT package based on FEFF 6.[4] Upon importing, data were rebinned with grids of 10 eV, 0.5 eV, and 0.05 $Å^{-1}$ for the pre-edge region, XANES region, and EXAFS region, respectively. Reference foil data were aligned to the first zero-crossing of the second derivative of the normalized μ(E) data, which was subsequently calibrated to the literature E_0 for the gold L_{III}-edge. Spectra were averaged in μ(E) prior to normalization. The background was removed and the data were assigned an Rbkg value of 1.2 prior to normalizing to obtain a unit edge step. Upon averaging, all data were aligned and processed simultaneously to afford identical values for the absorption edge energy (E_0), pre-edge range (125 to 30 eV below E_0), normalization range (150 to 980 eV above E_0), and spline range (0 to 980 eV above E_0).

All data were fit simultaneously with k-weighting of 1, 2, and 3 in R-space. A fit of Au foil was used to determine S_0^2 for all other samples. Structure models for all samples were obtained by considering the first two coordination shells of Au atoms and a multiple-scattering "rattle" path from the 1st coordination shell Au atom. Structural parameters that were determined by the fits include the degeneracy of the i^{th} scattering path (CN_i), the energy shift of the photoelectron (ΔE_0), and the mean square relative displacement of the i^{th} scattering element (σ_i^2). For the Au foil, coordination numbers were fixed based on the crystal structure. The change in effective scattering half-path length (ΔR_{eff}) for each scatterer was determined by assuming isotropic expansion of the Au nanoparticle. Accordingly, this isotropic scattering parameter (α) was multiplied by R_{eff} to afford ΔR_{eff}. Fitted parameters for all samples are provided in Table S1.

1.4 Catalytic CO oxidation

Catalytic CO oxidation was carried out in a fixed-bed reactor (straight quartz tube) at atmospheric

pressure. For the measurement of CO light-off curves showing CO conversion as a function of reaction temperature, a 20 mg catalyst supported by quartz wool was loaded in the reactor. The feed gas of 1 % CO balanced with dry air (< 4 ppm water) passed though the catalyst bed at a flow rate of 10 ml/min corresponding to gas hourly space velocity (GHSV) of 30,000 mL $(h\ g_{cat})^{-1}$. Prior to the catalytic test, each catalyst was calcined in an oven under air at 700 °C, 800 °C and 900 °C for 2 h. The concentrations of CO and CO_2 in the reactor effluent were analyzed by a Buck Scientific 910 gas chromatograph equipped with a dual molecular sieve/porous polymer column (Alltech CTR1) and a thermal conductivity detector. Steady-state CO oxidation was conducted with the same feed gas at 20 °C.

1.5 *In situ* infrared study

The adsorption of CO followed by FTIR spectroscopy was performed using a Thermo Nicolet Nexus 670 FTIR spectrometer with an MCT detector, while the effluent stream was monitored by a Pfeiffer Vacuum GSD 301 O2 mass spectrometer. Each spectrum was recorded with 32 scans at a resolution of 4 cm^{-1}. Each sample was loaded into a porous ceramic cup, and the cup was inserted into a DRIFTS cell (Pike Technologies DiffusIR). The sample was activated at 300 °C for 1 h under 30 ml/min flow of 4% H_2/Ar (Airgas). Subsequently, the temperature was decreased to 5 °C using a Fisher Scientific Isotemp 306S chiller before switching to He flow (30 ml/min). A background spectrum was collected, and the gas flow was switched to 30 ml/min of 2% CO/2% Ar/He for 10 min. During this period, a series of spectra were collected every 12.8 s during the adsorption of CO. After 10 min, the gas flow was switched to 30 ml/min of He for 10 min, and a series of spectra were collected every 12.8 s during the desorption of CO.

2. Figures

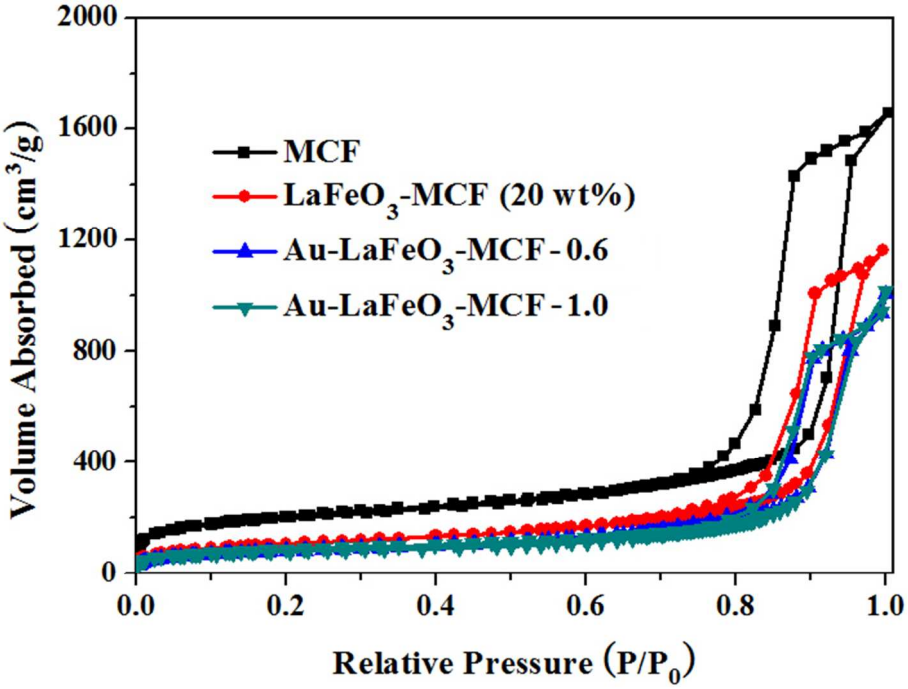

Figure S1. Nitrogen adsorption-desorption isotherms of MCF, $LaFeO_3$-MCF and the Au-$LaFeO_3$-MCF catalysts.

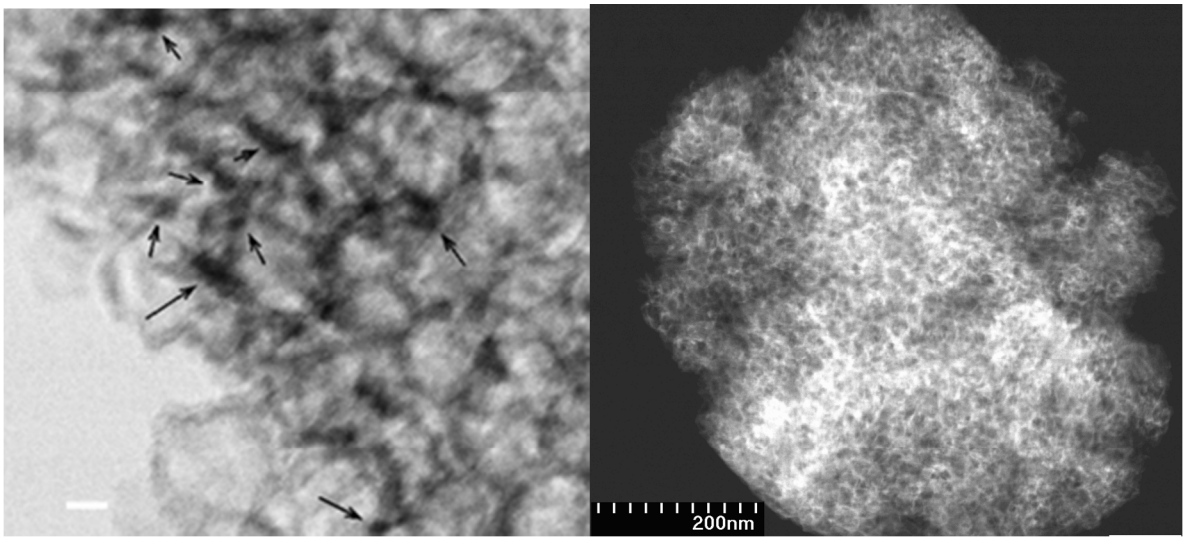

Figure S2. TEM and STEM images of $LaFeO_3$-MCF. Scale bar, 10 nm

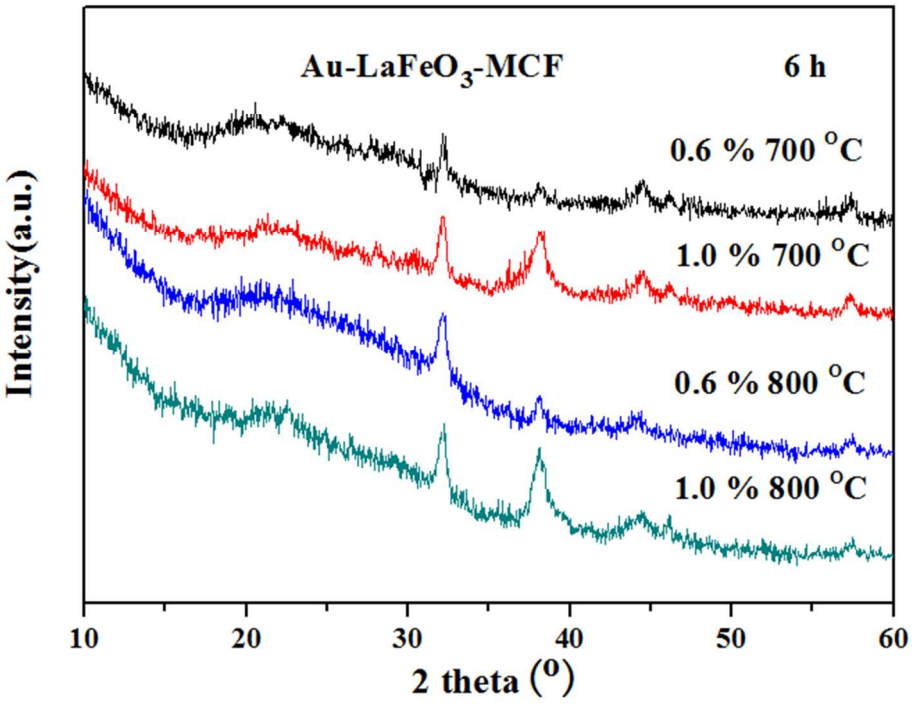

Figure S3. Wide-angle XRD patterns of the Au-$LaFeO_3$-MCF catalysts after calcination at different temperature for 6h.

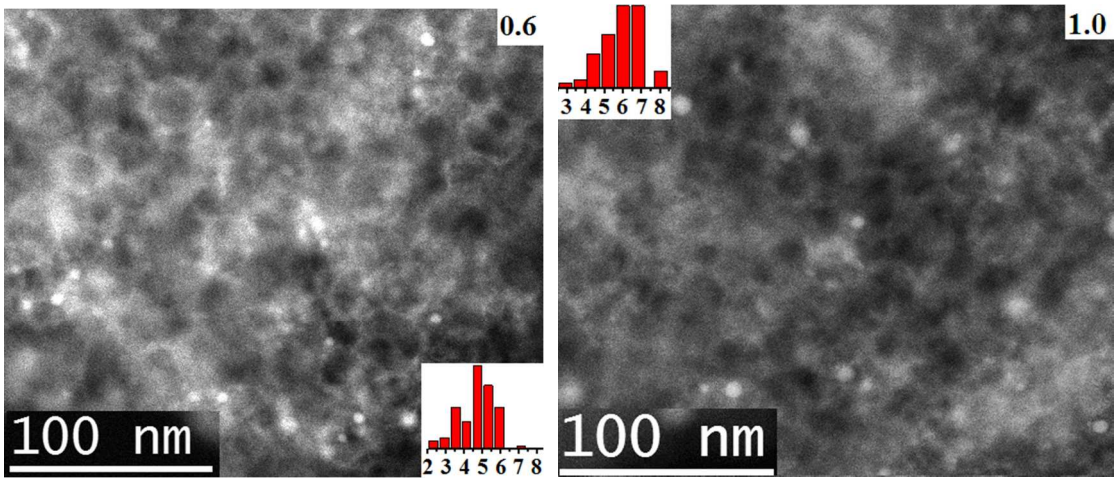

Figure S4. STEM images of the Au-$LaFeO_3$-MCF catalysts after calcination at 700 °C for 6h.

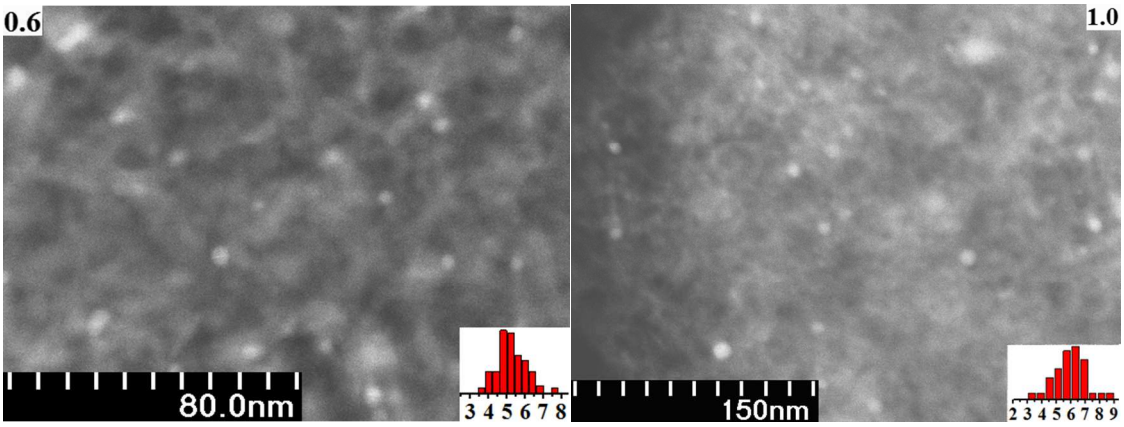

Figure S5. STEM images of the Au-$LaFeO_3$-MCF catalysts after calcination at 800 °C for 2h.

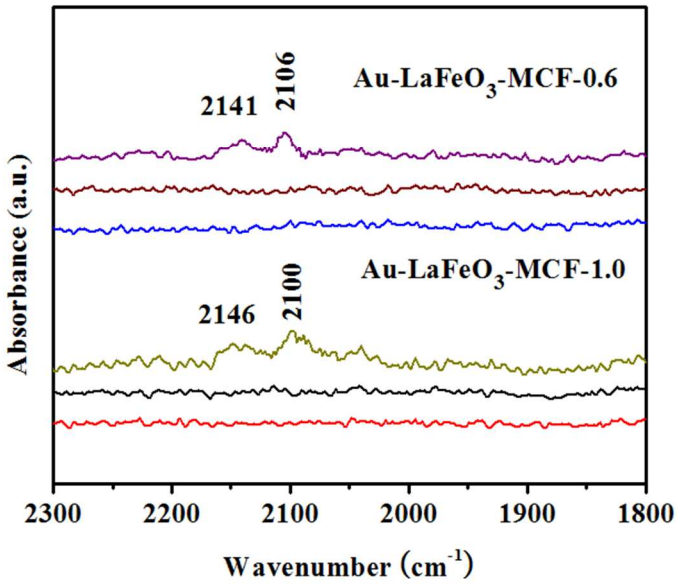

Figure S6. FTIR spectra of CO adsorption at 5 °C on the 800°C-calcined Au-$LaFeO_3$-MCF catalysts. In each group of spectra, the top spectrum was taken after 10 min of 2% CO flow with spectral contribution from gaseous CO subtracted. The middle and bottom spectrum were taken after purging the sample with He for 3 min and 10 min, respectively.

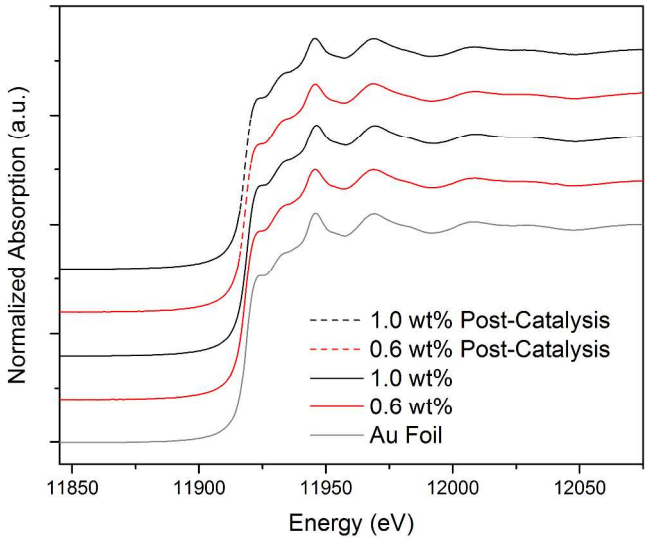

Figure S7. XANES data for Au L_{III}-edge. The solid grey line is the Au foil. Red lines correspond to data for 0.6 wt% Au-$LaFeO_3$-MCF before (solid) and after catalysis (dashed). Black lines correspond to data 1.0 wt% Au-$LaFeO_3$-MCF before (solid) and after catalysis (dashed).

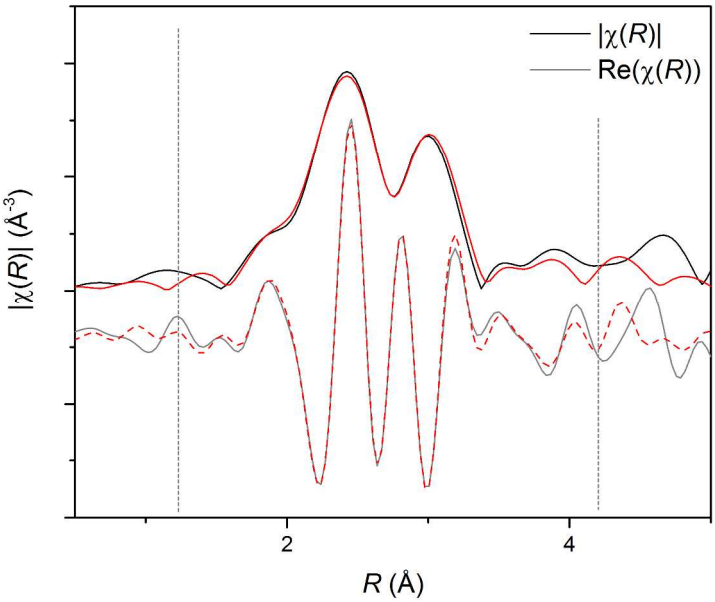

Figure S8. Au L_{III}-edge EXAFS spectrum and fit of Au foil. The magnitude of the Fourier transform of the experimental spectrum is displayed in solid black while the fit is displayed in solid red. The real component of the Fourier transform is plotted offset beneath in grey, with the fit displayed in dashed red.

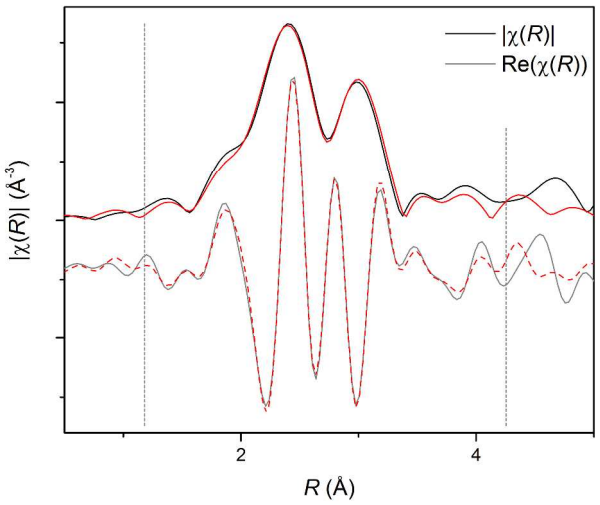

Figure S9. Au L_{III}-edge EXAFS spectrum and fit of 0.6 wt% Au-$LaFeO_3$-MCF after CO oxidation catalysis. The magnitude of the Fourier transform of the experimental spectrum is displayed in solid black while the fit is displayed in solid red. The real component of the Fourier transform is plotted offset beneath in grey, with the fit displayed in dashed red.

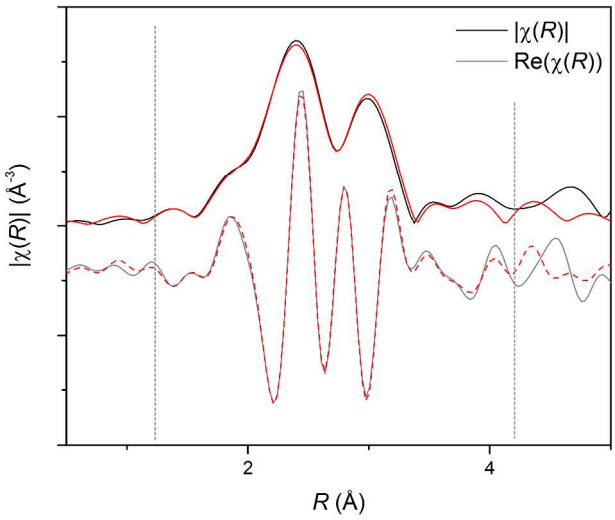

Figure S10. Au L_{III}-edge EXAFS spectrum and fit of 1.0 wt% Au-$LaFeO_3$-MCF after CO oxidation catalysis. The magnitude of the Fourier transform of the experimental spectrum is displayed in solid black while the fit is displayed in solid red. The real component of the Fourier transform is plotted offset beneath in grey, with the fit displayed in dashed red.

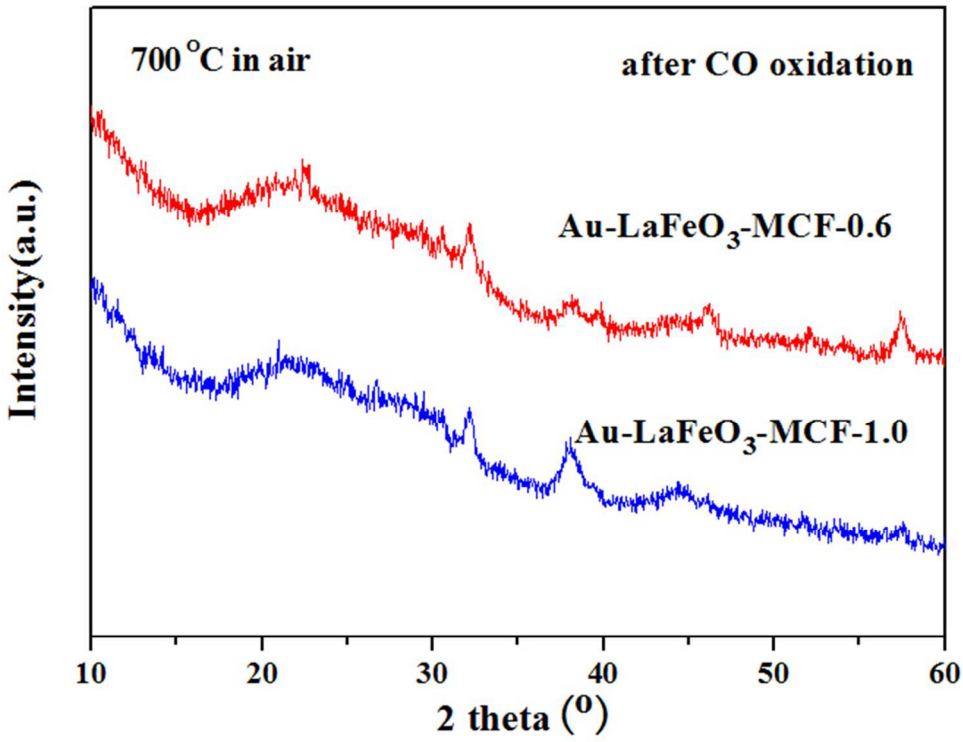

Figure S11. Wide-angle XRD patterns of the Au-$LaFeO_3$-MCF catalysts after CO oxidation.

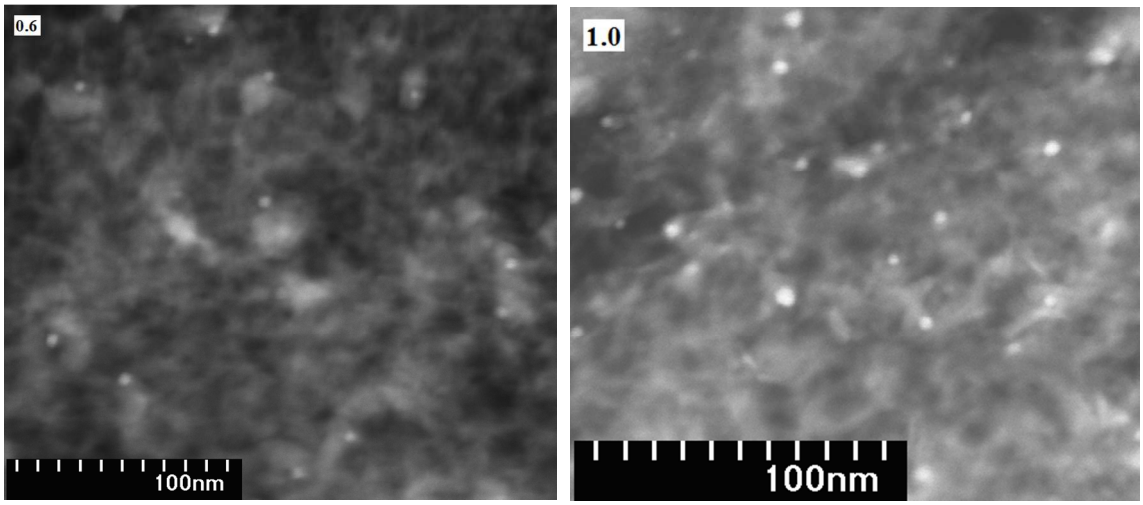

Figure S12. STEM images of the Au-$LaFeO_3$-MCF catalysts after CO oxidation.

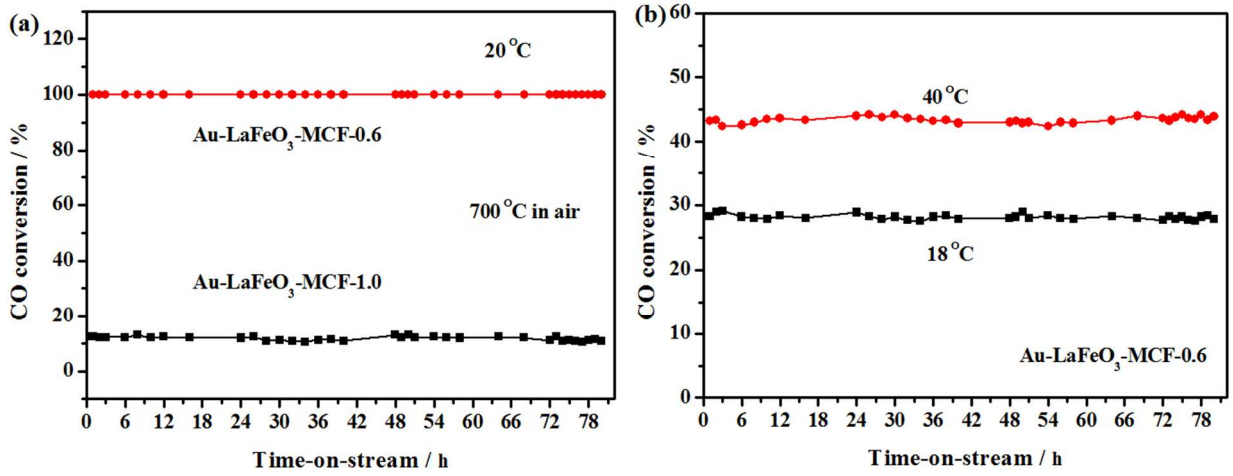

Figure S13. Time-on-stream of CO oxidation over (a) the Au-$LaFeO_3$-MCF catalysts at 20 °C (GHSV = 30000 mL (h gcat)$^{-1}$) and (b) the Au-$LaFeO_3$-MCF-0.6 catalyst at 18 °C and 40 °C (GHSV = 120000 mL (h gcat)$^{-1}$).

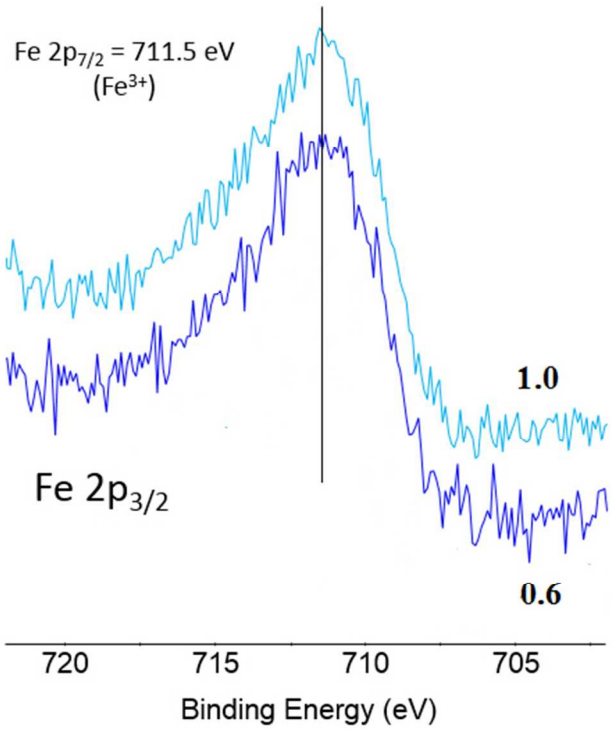

Figure S14. XPS spectra for Fe $2p_{3/2}$ of the Au-$LaFeO_3$-MCF catalysts.

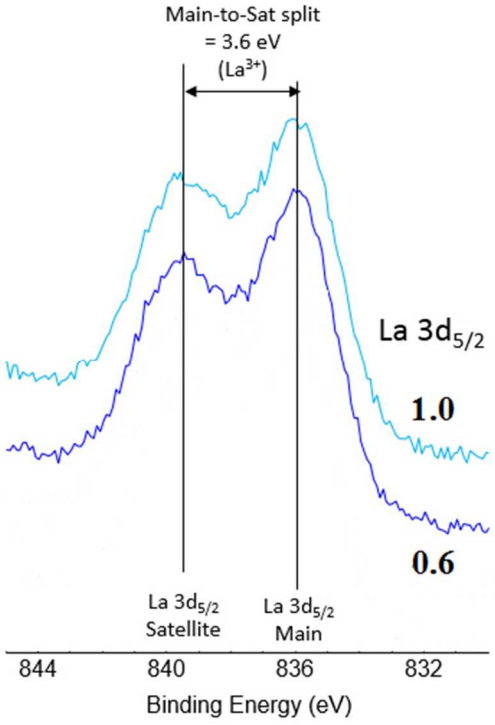

Figure S15. XPS spectra for La $3d_{5/2}$ of the Au-$LaFeO_3$-MCF catalysts.

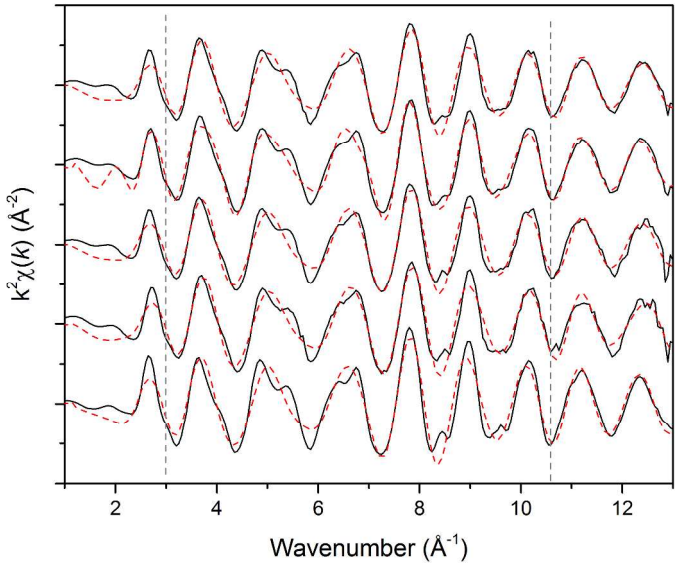

Figure S16. k^2-weighted χ(k) data and fits for EXAFS spectra collected at Au L_{III}-edge. Experimental data are in black, fits are in dashed red, and grey lines denote the fitting window. From bottom to top, spectra correspond to: Au foil, 0.6 wt% Au-$LaFeO_3$ pre-catalysis, 0.6 wt% Au-$LaFeO_3$ post-catalysis, 1.0 wt% Au-$LaFeO_3$ pre-catalysis, 1.0 wt% Au-$LaFeO_3$ post-catalysis. Data and fits are offset for ease of viewing.

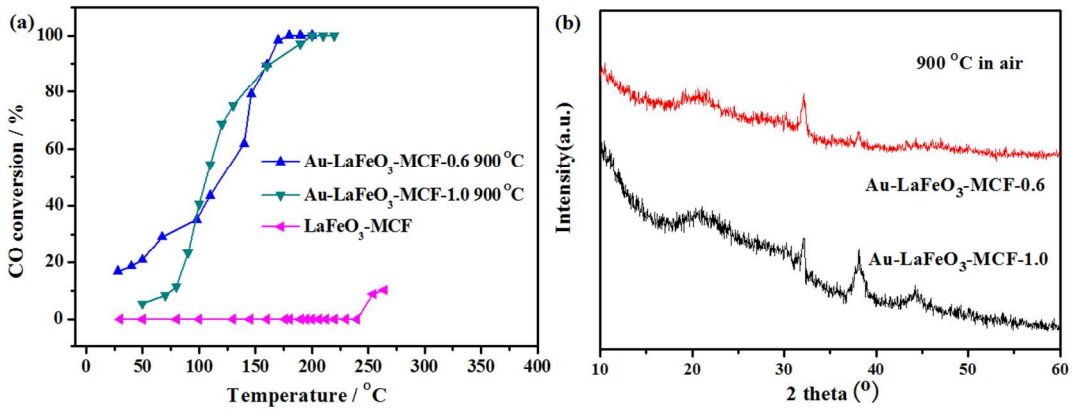

Figure S17. (a) CO light-off curves of $LaFeO_3$-MCF and the Au-$LaFeO_3$-MCF catalysts after calcination at 900 °C in air for 2h. (b) Wide-angle XRD patterns of the Au-$LaFeO_3$-MCF catalysts after calcination at 900 °C.

3. Tables

Table S1. Fitted parameters for Refined Au EXAFS fits.

Parameter	**Au foil**	**0.6 wt% Au-$LaFeO_3$-MCF**		**1.0 wt% Au-$LaFeO_3$-MCF**	
		Pre-Catalysis	*Post-Catalysis*	*Pre-Catalysis*	*Post-Catalysis*
S_0^2	0.790 ± 0.6	0.790[a.]	0.790[a.]	0.790[a.]	0.790[a.]
E_0 (eV)	5.1 ± 0.5	5.3 ± 0.4	4.5 ± 0.5	5.0 ± 0.4	4.6 ± 0.5
α ($\times 10^{-3}$)	-7 ± 2	-12 ± 1	-11 ± 2	-10 ± 1	-11 ± 1
σ_1^2 ($\times 10^{-3}$ Å^2)	7.6 ± 0.7	8.3 ± 0.5	8.5 ± 0.8	8.1 ± 0.5	8.1 ± 0.7
σ_2^2 ($\times 10^{-3}$ Å^2)	11 ± 2	3 ± 7	10 ± 10	4 ± 6	8 ± 8
N_{IDP}	15	13	14	13	14
N_{Var}	5	6	6	6	6
R	1.4 %	0.7 %	1.3 %	0.5 %	0.9 %
Nanoparticle Radii (nm)		3.12	3.12	3.39	2.90

a. Fixed value determined from fit of Au foil spectrum.

4. References

(1) (a) Schmidt-Winkel, P.; Lukens, W.W.; Zhao, D.; Yang, P.; Chmelka, B.F.; Stucky, G.D. *J. Am. Chem. Soc.* **1999**, 121, 254-255. (b) Schmidt-Winkel, P.; Lukens, W.W.; Yang, P.D.; Margolese, D.I.; Lettow, J.S.; Ying, J.Y.; Stucky, G.D. *Chem. Mater.* **2000**, 12, 686-696.

(2) Yan, W.F.; Brown, S.; Pan, Z.W.; Mahurin, S.M.; Overbury, S.H.; Dai, S. *Angew. Chem. Int. Ed.*, 2006, 45, 3614-3618.

(3) Segre, C. U.; Leyarovska, N. E.; Chapman, L. D.; Lavender, W. M.; Plag, P. W.; King, A. S.; Kropf, A. J.; Bunker, B. A.; Kemner, K. M.; Dutta, P.; Duran, R. S.; Kaduk, J. In *The MRCAT Insertion Device Beamline at the Advanced Photon Source*, Synchrotron Radiation Instrumentation: Eleventh U.S. National Conference, New York, NY (USA), Pianetta, P., Ed. American Institute of Physics: New York, 2000; Vol. 521, p 419.

(4) (a) Ravel, B.; Newville, M., ATHENA, ARTEMIS, *J. Synchrotron Radiat.* **2005**, 12, 537-541. (b) Rehr, J. J.; Albers, R. C., *Rev. Mod. Phys.* **2000**, 72, 621-754.